

Aerodynamic loading acting on the stator vane in the variable nozzle turbine flow

M. Žatko^{a,*}

^aFaculty of Mechanical Engineering, University of Technology in Brno, Technická 2896/2, 616 69 Brno, Czech Republic

Received 4 January 2015; received in revised form 6 May 2015

Abstract

The purpose of this paper is to evaluate an aerodynamic loading acting on the stator vanes of the turbocharger using variable nozzle turbine (VNT). Computational fluid dynamic (CFD) is applied using commercial software ANSYS CFX. A full turbine stage CFD model is used to investigate the aerodynamic loading in several operating points for different stator vane positions. Results are compared with the measurement on the Gas Stand testing rig. This device burns natural gas and produces a stable flow at very high temperatures. This excludes the impact of the engine control management, the engine vibrations, and the flow pulsations on measured values. A comparison of measured and simulated vane aerodynamic loading provides a very good correlation. These encouraging results show a high potential of CFD methods for further development and optimization of VNT mechanism.

© 2015 University of West Bohemia. All rights reserved.

Keywords: turbocharger, stator vane, VNT, aerodynamic loading, CFD

1. Introduction

Demands on emission limits for modern automotive engines cause that turbocharged engines became a standard across the diesel market and started to penetrate the gasoline market as well. Challenging requirements on the engines air management leads to a promotion of variable nozzle turbines, which combine a volute with a row of movable stator vanes with a rotating axis parallel to the turbine axis. Stator vanes allow driving the throat area and the incidence angle to the turbine wheel. This helps to fulfil engine boost demands at low engine speeds and transient runs. Opening of the VNT mechanism decreases the turbine pressure ratio, which protects the engine from over-boosting. Several researches pointed out the advantages of the VNT design. Baines and Lavy [1] compared a turbine performance with vaned and vaneless stators. The authors observed that the vaned stator delivered the improved efficiency across the range of comparison together with the improvement of engine transient performance. Common problems encountered with the VNT were reliability, caused by a long time period of exposition to a high temperature and corrosive exhaust gases, complexity of the VNT actuation mechanism and subsequently high cost [6]. Many of these problems have already been sufficiently solved but the intention to achieve a lower price together with demands on emission limits encourage the efforts to improve the existing solutions. This leads to the promotion of rotary electric actuators (REA) which provide a very precise controllability of the stator vane position and also an improved reliability. Requirements on the REA performance, which are expected to handle aerodynamic loading of vanes and friction forces in the whole kinematic mechanism, and packaging issues, which rapidly restrict a usable design space, lead to a challenging and expensive development process of these

*Corresponding author. Tel.: +420 777 522 948, e-mail: miroslav.zatko@gmail.com.

actuators. One method of how to reduce these requirements is to understand and optimize the aerodynamic loading of stator vanes. Increasing computational power and software capability offer an opportunity to investigate this loading using CFD methods. Several computational studies focused on vane aerodynamic loading have been conducted in the past [2, 3]; however none of them was verified by direct measurement. This paper is focused on the investigation of aerodynamic loading during several turbocharger operation regimes and boundary conditions, with the following experimental verification of the results. An experimental device is introduced to perform in situ measurements of aerodynamic loading with the use of the Gas Stand device. This burns natural gas producing a very stable flow condition at very high temperatures. It excludes the impact of the engine control management, the engine vibrations and the flow pulsations on measured values.

2. Numerical model

The computations are performed using ANSYS CFX software. A full turbine stage model is created; this consists of four parts: volute, vane passage, turbine wheel, and outlet extension (see Fig. 1). Each of them is meshed separately.

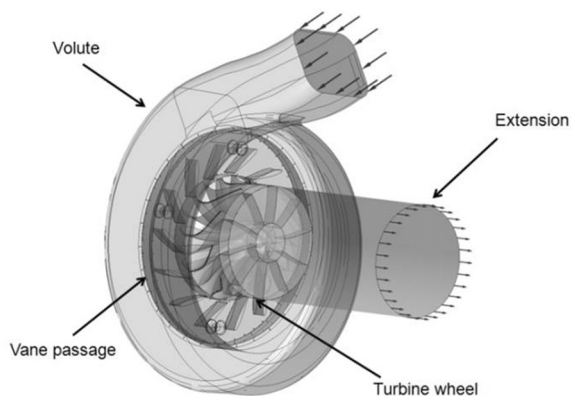


Fig. 1. Turbine stage geometry model

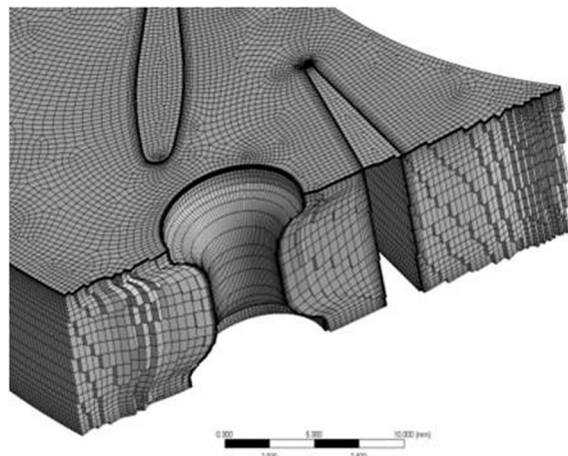


Fig. 2. Vane passage hexagonal grid with side clearance

The mesh for volute is created using an unstructured tetrahedral grid due to complexity of its geometry. Prismatic cells in near wall regions are created to properly solve the flow in boundary layers. These consist of eight prism layers with expansion ratio 1.2. The grid is refined in the high curvature areas especially around the volute tongue. Hence the main focus of this paper is the stator vane aerodynamic loading, vane passage domain is highly refined. The structured hexahedral grid is created using the sweep method, including the 0.15 mm vane side clearance on the hub side. This consists of five layers of hexahedral elements and it is conformably connected to the rest of the domain (see Fig. 2). Several grid configurations are set up in the grid independence study to find out the best trade off between the computational time and precision. The results are presented in Table 1. Configuration number four was selected. This provides grid refinement around the stator vanes using twelve prism layers with 1.2 expansion ratio, to create a very smooth transition from the near wall region to the rest of computational domain (see Fig. 2). The mesh of the turbine wheel rotational domain is created using TURBOGRID meshing software. The structured hexahedral grid using H/J/C/L-topology definition and O-grid wrapped around the blade is used.

Table 1. Grid independence study

Grid configuration	Number of elements	Max element size [mm]	Mass flow rate [kgs ⁻¹]	Temperature Outlet [°C]	Vane Force [N]	Vane Torque [Nmm]	Time per 100 iteration [h]
1	2 973 877	0.750	0.439	543.9	11.50	−19.41	0.63
2	3 501 167	0.500	0.440	543.8	11.49	−19.11	0.86
3	4 366 507	0.375	0.440	543.8	11.46	−18.93	1.07
4	5 253 382	0.300	0.440	543.8	11.44	−18.88	1.76
5	6 529 472	0.250	0.440	543.8	11.44	−18.88	2.20

A two-equation SST turbulence model developed by Menter [4] is used in this study. This is generally a preferred turbulence model in turbo machinery applications used by many researchers. It is based on the eddy viscosity approximation where the turbulence is assumed to consist of small eddies continuously formed and dissipated, in which Reynolds stresses are assumed to be proportional to the mean velocity gradients. Used in conjunction with a scalable wall function approach, the SST turbulence model can be applied to arbitrarily fine grids, with the model switching from a standard log-law approximation of the boundary layer profile to a low Reynolds number calculation depending on the local grid resolution [5].

The boundary conditions consist of the total pressure and temperature at the volute inlet and the static pressure at the extension outlet area. For the turbine wheel rotational domain, the rotational speed is specified. The reference pressure is assumed as 0 Pa; thus all pressures are modelled as absolute pressures. A stage rotor/stator interface is used to connect the rotational domain with the rest of the model. This performs a circumferential averaging of the fluxes through the bands on the interface and is commonly used in turbo machinery.

An ideal air gas model with modified specific heat capacity at constant pressure, corresponding to the gas stand conditions, is used as a material model for all domains. A total energy heat transfer model that includes the viscous work term is selected and all walls are modelled as no slip, adiabatic walls. Computations are performed using the high resolution advection scheme and the first order turbulence numerics. A physical time step option, related to the rotational speed of the turbine wheel is set up, using the following expression $t = 1/\omega$, where ω is the turbine wheel rotational speed. For each case, the target value of the RMS residuals is set to 10^{-5} . This is typically reached after 150–200 iterations and provides a stable behaviour of monitored variables.

3. Vane aerodynamic loading

The evaluation of vane aerodynamic loading is based on the pressure distribution of vane profile. Aerodynamic force and torque are calculated in the vane local coordinate system presented in Fig. 3. This is placed in the pivot point of the vane. The x -axis is a connection between the pivot point and the vane trailing edge. The z -axis is directed to the outlet extension, which means that the negative torque value tends to open the vane. For the simplification of the evaluation process, the vane torque represents torque around the z -axis (torque x and y are assumed as negligible) and the vane force represents the magnitude of the force. This component of loading is used to estimate additional friction torque acting on the vane shaft. A definition of the vane angle

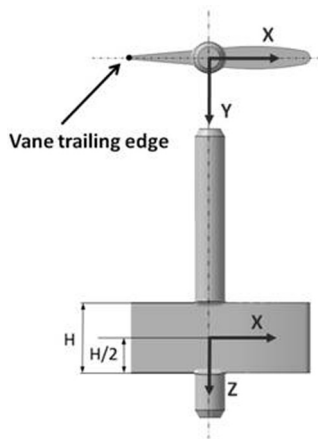


Fig. 3. Vane local coordinate system

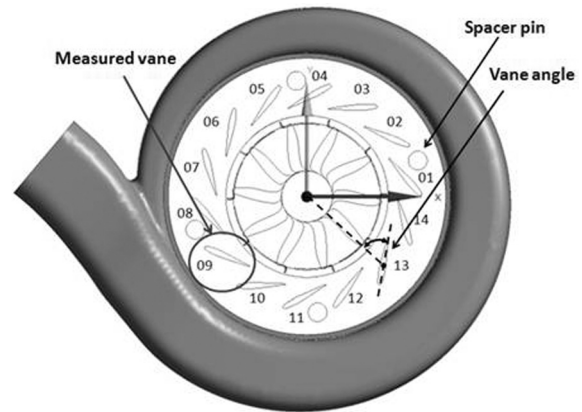


Fig. 4. Vane numbering & spacer pin positions

is presented in Fig. 4. This is an angle between the x -axis of the local vane coordinate system and a connection between the vane pivot point and the turbocharger rotation axis. Hence the VNT turbocharger works at large range of boundary conditions; three referral vane positions are selected. It is a minimal vane open position at 84.66 deg vane angle, medium open position at 61.62 deg and maximal vane open position at 40.78 deg vane angle. These three vane positions are also used for experimental validation of the model.

The global pressure distribution is investigated for each of these vane positions along with the analysis of aerodynamic loading presented for the four selected vanes: 2, 7, 11, and 14. These represent circumferential differences across the volute (see Fig. 4). A special attention is paid to the vane number nine which was used during the experimental validation of the calculations. For this particular vane the influence of three different pressure ratios to the vane aerodynamic loading is presented. The rotational speed of the turbine wheel and the turbine inlet temperature remain the same and the outlet static pressure is assumed as 100 kPa. This comparison is made for all three vane positions. Several researchers pointed out the influence of spacer pins on vane aerodynamic loading [2, 3]. These pins are used to assemble the stator rings and to ensure the constant stator channel width. A position of these pins is presented in Fig. 4. Hence there are four spacer pins in the investigated stator; it can be assumed that it will have a significant influence on the vane aerodynamic loading, especially on the affected vane couples: 1&2, 4&5, 8&9, 11&12. Therefore all simulation cases are modelled and compared with and without spacer pins. All figures presented in the following study are plotted for pressure ratio of four and a mid span plane position.

Minimal vane open position

This vane position is characteristic by a very small vane to vane distance. A decreased throat area results in the high pressure gradient in the stator streamwise direction. Vanes create small nozzles, transforming the pressure energy to the kinetic energy with a high circumferential velocity component. This results in increased shaft work even for the low engine mass flow rates. A pressure distribution across the volute is presented in Fig. 5. This is homogenous in the volute circumferential direction. It can be seen that the influence of the volute shape on the vane aerodynamic loading in this vane position is very small. A comparison of the aerodynamic force for each stator vane is presented in Fig. 6; this demonstrates a very even force distribution with the averaged value of 36 N and the maximum deviation from the average less than 1 %.

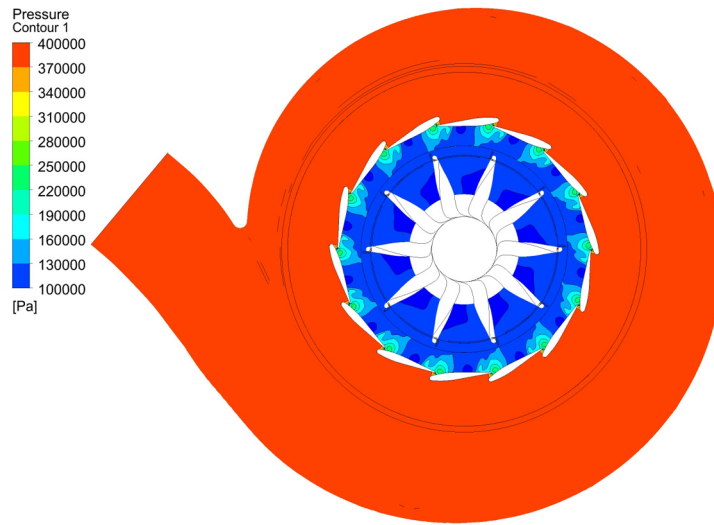


Fig. 5. Pressure contours: min open (PR 4)

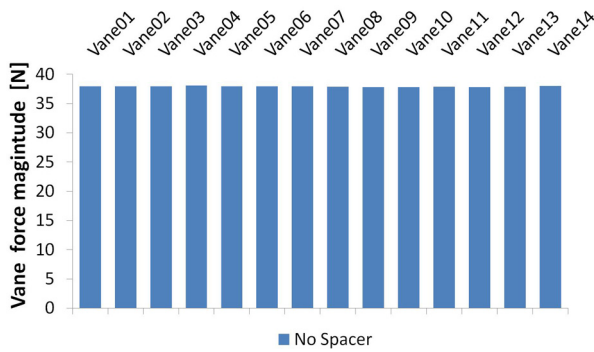


Fig. 6. Vane force distribution: min open (PR 4)

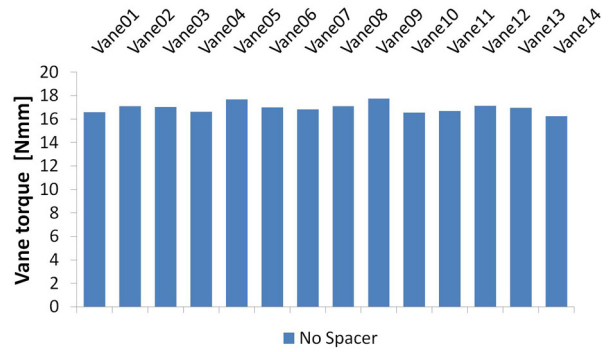


Fig. 7. Vane torque distribution: min open (PR 4)

The same behaviour could be observed in Fig. 7, where the distribution of aerodynamic torque is shown; averaged value is 17 Nmm with the maximum deviation less than 2 %.

The pressure distribution for the selected vanes is presented in Fig. 8. This is very same for each of these vanes. A very high pressure gradient between the vane suction and pressure side results in high aerodynamic force. However, the pressure distribution is balanced related to the vane pivot point; resulting in reduced aerodynamic torque.

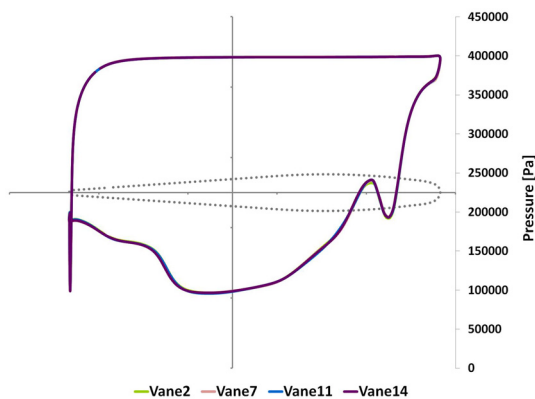


Fig. 8. Vane pressure distribution: min open (PR 4)

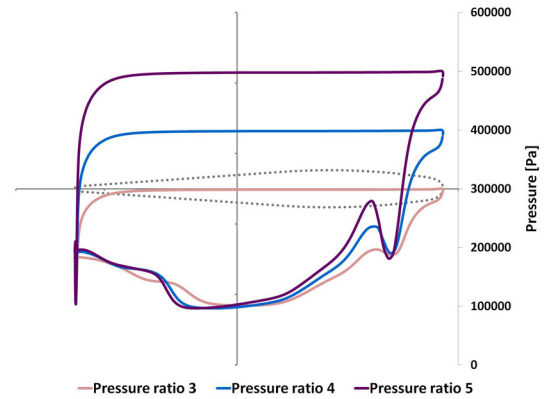


Fig. 9. Vane pressure distribution comparison

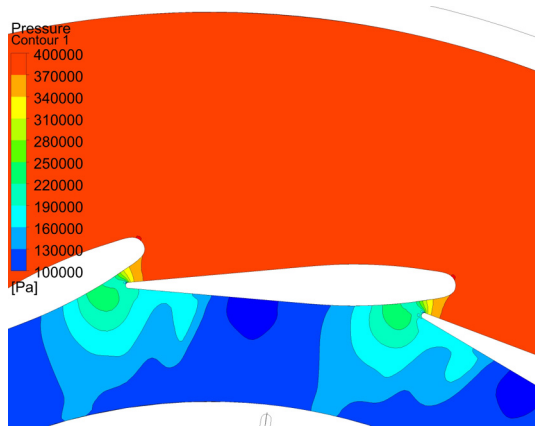


Fig. 10. Pressure contours: min open (PR 4)

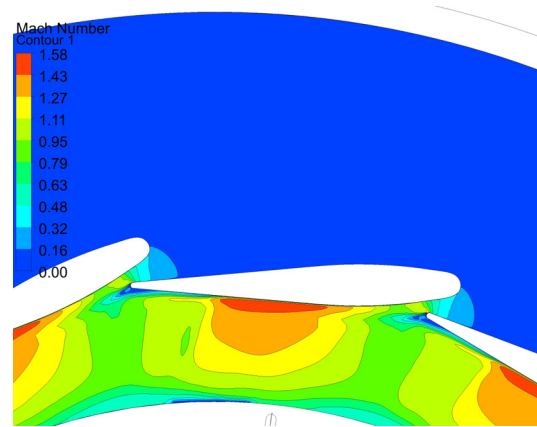


Fig. 11. Mach number contours: min open (PR 4)

A comparison of the vane pressure distribution around the vane number nine for three different pressure ratios is presented in Fig. 9. It can be seen that the pressure at the outlet of the stator is very close to the atmospheric pressure (see Fig. 10) and it is the same for all three pressure gradients. This effect is related to the low mass flow rate, which causes a low degree of the turbine wheel reaction. Contours of Mach number are presented in Fig. 11; the maximum Mach number is close to 1.6, which leads to a conclusion that the stator works in the transonic regime.

Spacer pin impact

The minimal vane open position is characteristic by high gas pressure energy and low gas kinetic energy before the flow enters the stator. This leads to an assumption that the influence of the spacer pins in this vane position is very low. The comparison presented in Fig. 13 shows the vane aerodynamic torque for the model with and without spacer pins. The difference is in averaged less than 2 %, thus the influence of spacer pins in this vane position could be assumed as negligible. This also confirms the comparison of the pressure distribution for the vane number nine presented in Fig. 12.

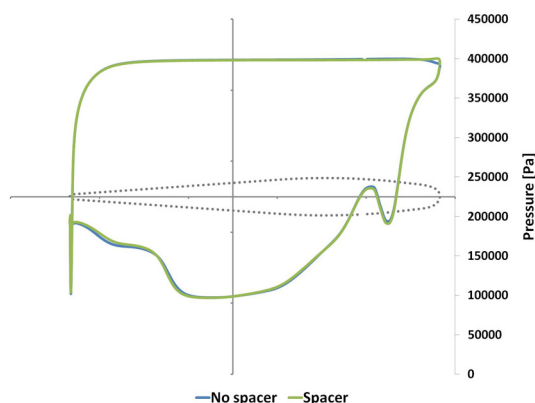


Fig. 12. Spacer pin influence: min open (PR 4)

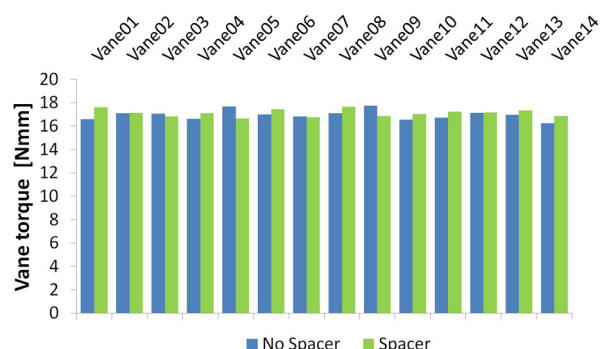


Fig. 13. Vane torque comparison: min open (PR 4)

Medium open vane position

This vane position is from the perspective of turbocharger operating conditions one of the most common regimes. The turbine stage pressure distribution is presented in Fig. 14.

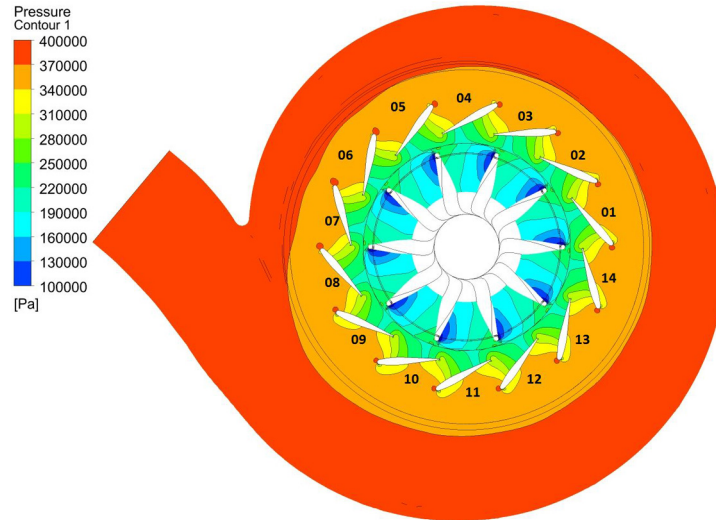


Fig. 14. Pressure contours: mid open (PR 4)

This shows an uneven pressure distribution in stator circumferential direction, which indicates that part of the expansion process is performed in the volute. This results in uneven distribution of the vane incidence angles and subsequently in different vane aerodynamic loading. The distribution of vane forces and torques across the volute without spacer pins is presented in Figs. 15 and 16.

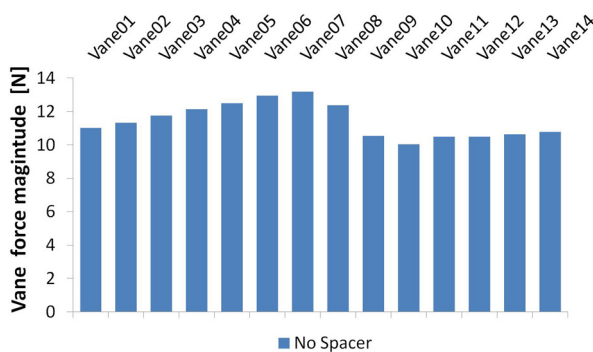


Fig. 15. Vane force distribution: mid open (PR 4)

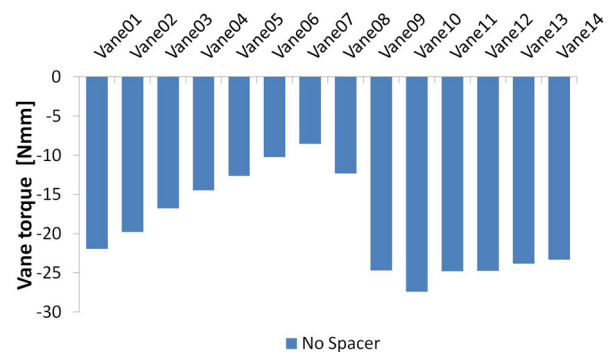


Fig. 16. Vane torque distribution: mid open (PR 4)

Maximum torque acts on the vane number ten located at the turbine inlet section. As the vanes are farther from the turbine inlet location, vane torque decreases and reaches its minimum value at the volute tongue location (vane number seven). An opposite trend is valid for the aerodynamic force; this reaches its maximum value at the vane number seven and decreases in circumferential direction with the opposite sense to the aerodynamic torque. This behaviour indicates that the vectors of the aerodynamic force acting on the vanes are shifted across the stator circumferential direction, reducing the arm to the vane pivot point.

The pressure distribution for four selected vanes is presented in Fig. 17; an increasing pressure difference from 10 to 50 % of vane chord length explains the maximum force acting on

the vane number seven. On the other hand, a smaller negative pressure difference from 0 to 10 % of vane chord length, acting on the large arm related to the vane pivot point, is responsible for lower aerodynamic torque. A comparison of the pressure distribution around the vane number nine for three different pressure ratios shows a scale and shift linear to the pressure ratio (see Fig. 18); corresponding pressure contours for pressure ratio of four are presented in Fig. 19.

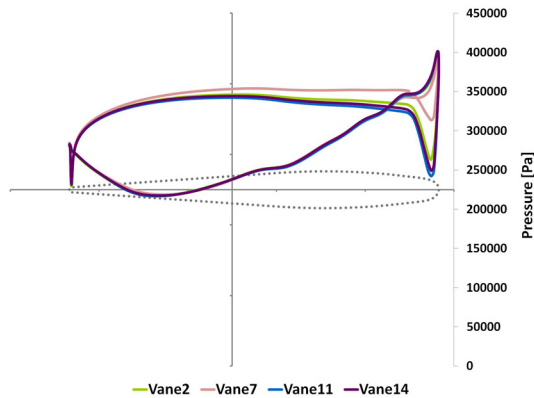


Fig. 17. Vane pressure distribution: mid open (PR 4)

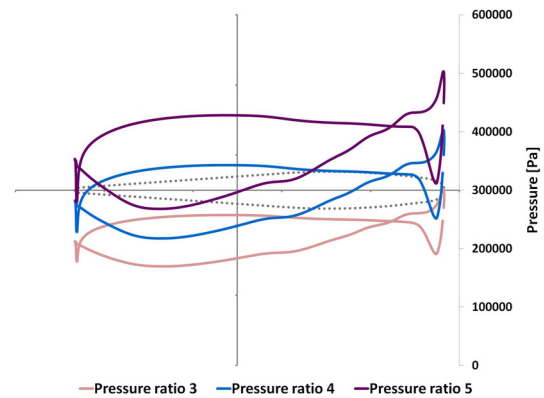


Fig. 18. Vane pressure distribution comparison

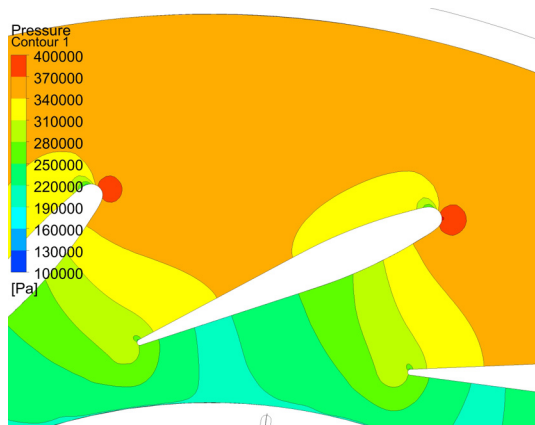


Fig. 19. Pressure contours: min open (PR 4)

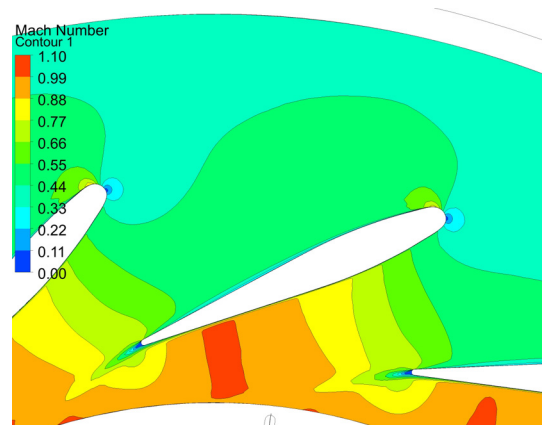


Fig. 20. Mach number contours: min open (PR 4)

Mach number contours presented in Fig. 20 indicate that the stator in this position works mostly under subsonic conditions, with velocity corresponding to the Mach number up to 1.1.

Spacer pin impact

The comparison of aerodynamic loading for the stator with and without spacer pins is presented in Figs. 21 and 22. It can be observed that the spacer pins have a significant impact on the vane torque; this is decreased on the first vane of the affected vane couple and reversed on the second one (vanes number 2, 5, 9, 12). On the other hand, the comparison of aerodynamic forces shows approximately 15 % increase in the force for these vanes. The comparison of the pressure distribution for the vane number nine explains this phenomenon. The spacer pins reverse the pressure difference located at 10 % of vane chord length. This change acts on the large arm related to the vane pivot point, which results in the opposite sense of resulting vane torque (see Fig. 23). Pressure contours presented in Fig. 24 illustrate this phenomenon and show a huge impact of the spacer pin on the nearest vane couple.

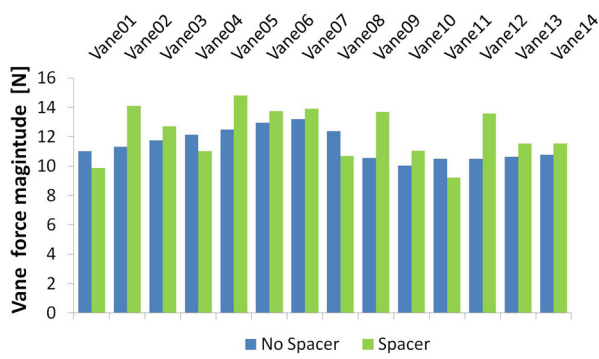


Fig. 21. Vane force comparison: mid open (PR 4)

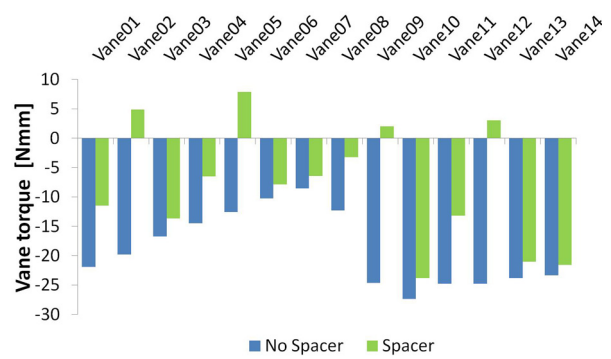


Fig. 22. Vane torque comparison: mid open (PR 4)

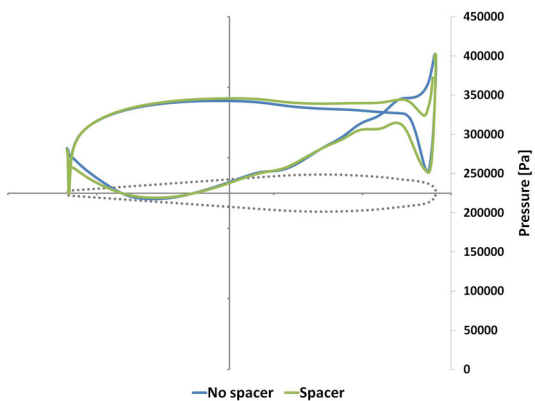


Fig. 23. Spacer pin influence: mid open (PR 4)

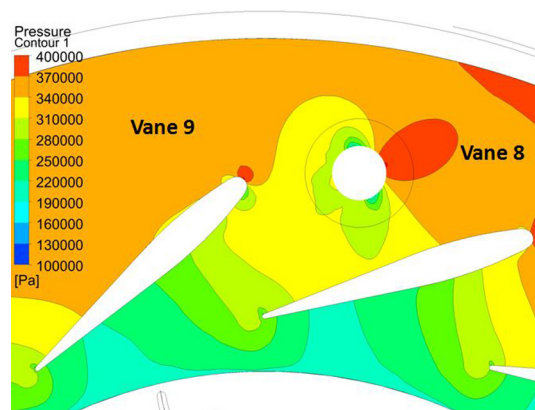


Fig. 24. Spacer pin pressure contours: mid open (PR 4)

Maximal vane position

This vane position is characteristic by a very high throat area and high mass flow rate. It is used to protect the turbine against over-revving, by decreasing the turbine pressure ratio. A pressure distribution across the volute is presented in Fig. 25.

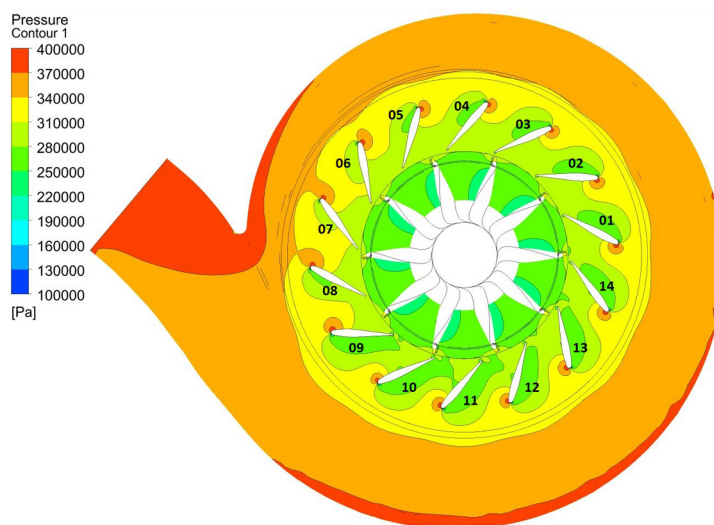


Fig. 25. Pressure contours: max open (PR 4)

This is significantly uneven, resulting in different flow incidence angles in stator circumferential direction. The comparison of aerodynamic forces is illustrated in Fig. 26, which shows a dramatically uneven distribution. Forces reach their minimum value at the volute tongue area (vane number seven); then the value rapidly increases near the volute inlet area. From there the values are decreasing in the stator circumferential direction. On the other hand, a distribution of the aerodynamic torques presented in Fig. 27 shows uniform values, except of the volute tongue-inlet area. This leads to a conclusion that the uneven distribution of aerodynamic forces is compensated by distribution of arms related to the vane pivot points. Even if the magnitude of the forces is in comparison with the previous cases relatively small, the aerodynamic torques reach their maximum values in the opening sense of rotation. The vane pressure distribution in Fig. 28 shows that the acting pressure at the pressure side of the vane profile is lower than the pressure acting on the suction side at 95 % of the whole vane chord. This results in the lifting force which tends to open the vane. A peak of pressure at 5 % of vane chord length is acting on the large arm, which explains the high value of aerodynamic torque, even for a small force. A pressure distribution for the vane number seven shows a balanced pressure difference, which explains its very low force (see Fig. 28). On the other hand, the pressure distribution for the vane number nine presented in Fig. 29 shows a large difference between the vane pressure and suction side, resulting in a significantly higher force. This effect is scaled and shifted for each of the investigated pressure ratio. Corresponding pressure contours around the vane number nine for pressure ratio of four are presented in Fig. 30. The force reversal effects in this vane position are caused by a large flow separation visible on Mach number contours presented in Fig. 31. This is caused by a very high vane angle and a high mass flow rate typical for this vane position.

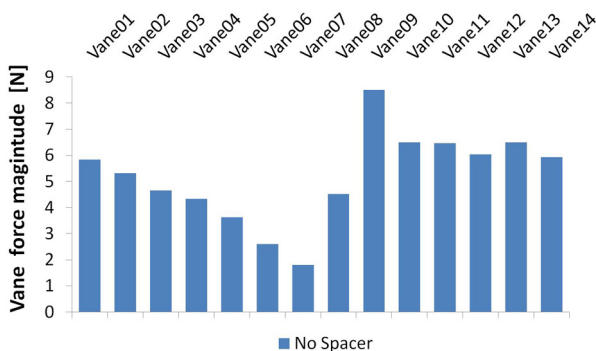


Fig. 26. Vane force distribution: max open (PR 4)

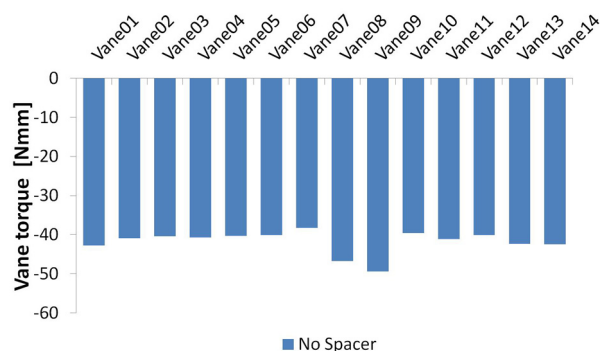


Fig. 27. Vane torque distribution: max open (PR 4)

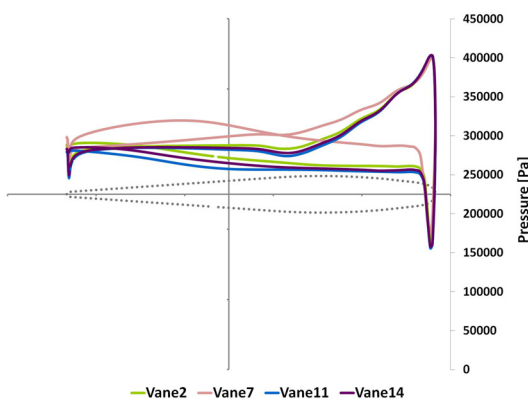


Fig. 28. Vane pressure distribution: max open (PR 4)

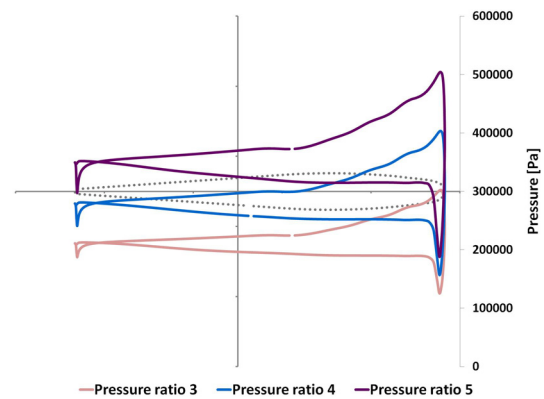


Fig. 29. Vane pressure distribution comparison

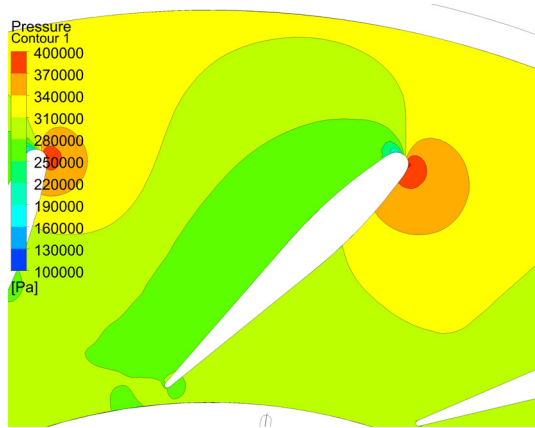


Fig. 30. Pressure contours: max open (PR 4)

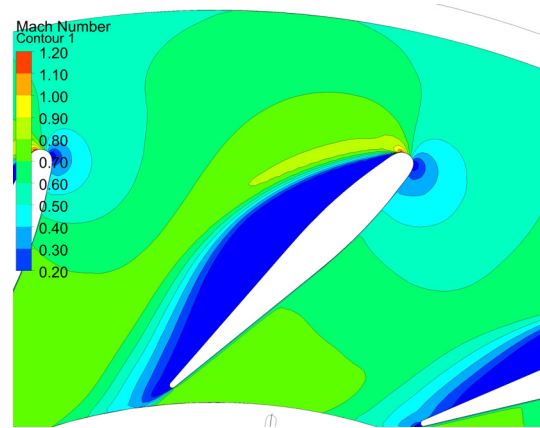


Fig. 31. Mach number contours: max open (PR 4)

Spacer pin impact

The comparison of aerodynamic loading for this vane position with and without the spacer pins is presented in Figs. 32 and 33. Aerodynamic forces and torques on the second vane of the influenced couples is significantly reduced (vanes number 2, 5, 9, 12).

The spacer pins reduce the active channel area between affected vanes, which results in increased speed and decreased static pressure acting on the suction side of the affected vanes. This is clearly visible in the comparison of pressure distribution in the vane number nine presented in Fig. 34. A blocking effect of the spacer pin acting on the vane number nine is also visible on the pressure contours presented in Fig. 35.

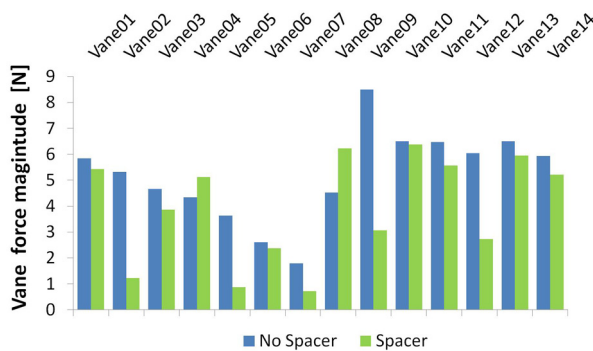


Fig. 32. Vane force comparison: max open (PR 4)

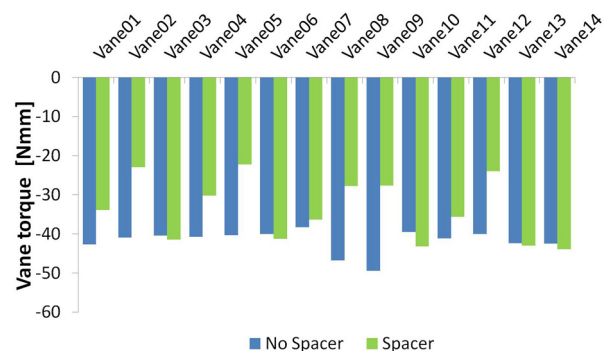


Fig. 33. Vane torque comparison: max open (PR 4)

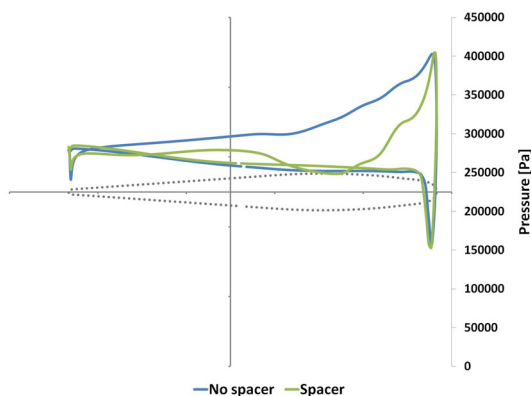


Fig. 34. Spacer pin influence: max open (PR 4)

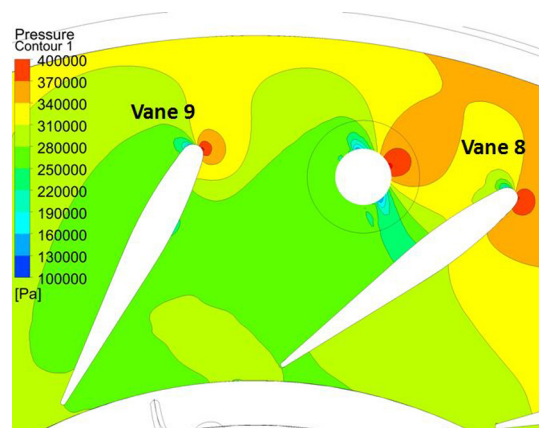


Fig. 35. Spacer pin pressure contours: max open (PR 4)

4. Summary of simulation results

The results of full stage CFD simulation show a significant influence of the vane circumferential position inside the volute, related to the turbine inlet and to the turbine tongue, on the resulting aerodynamic loading. However, global trends for vane averaged aerodynamic loading presented in Fig. 36 show a linear behaviour for the investigated range of pressure ratios. Maximum of the aerodynamic forces is reached at minimal vane open position, with a very steep slope of the curve. This is caused by very high pressure gradient between the vane pressure and suction side. However, the resulting force is significantly reduced by the arm related to the vane pivot point, which leads to relatively low aerodynamic torque (see Fig. 37).

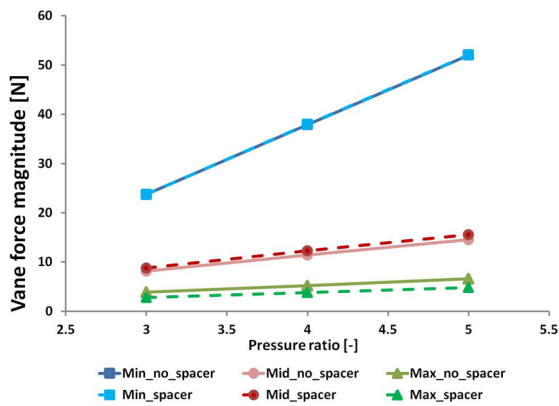


Fig. 36. Averaged vane force vs. pressure ratio

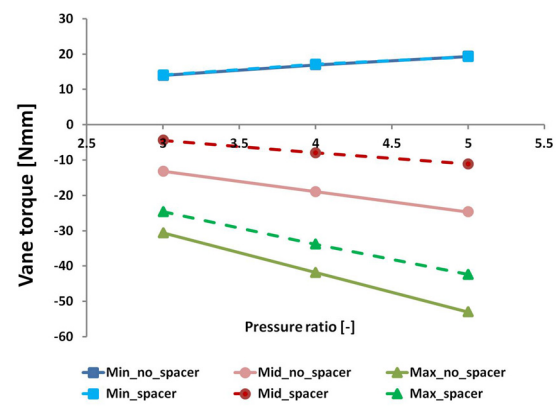


Fig. 37. Averaged vane torque vs. pressure ratio

On the other hand, a relatively low aerodynamic force, acting in the maximal vane open position, is multiplied by very high arm. This results in maximum values of aerodynamic torque. The simulation outputs also highlighted a very high influence of the spacer pins location, especially for medium and maximal vane open positions. The spacer pins significantly change the vane pressure distribution, which leads to lower vane torque (see Fig. 37). The comparison of the aerodynamic force in dependence on the vane angle is presented in Fig. 38 which shows a significant non-linearity at the vane operating range. On the other hand, the vane aerodynamic torque presented in Fig. 39 seems to be linear with change of the sense of rotation close to 70 deg vane angle.

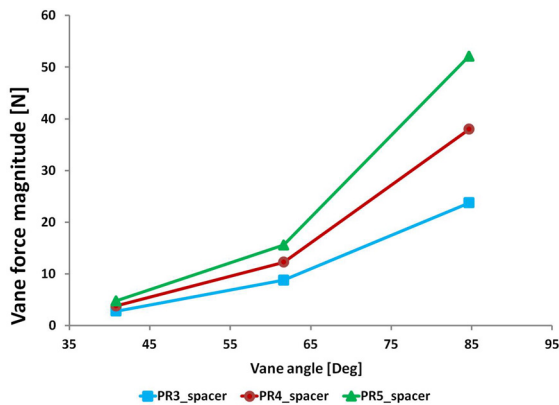


Fig. 38. Averaged vane force vs. vane angle

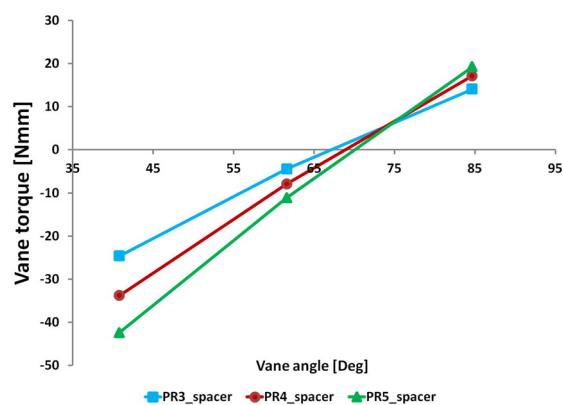


Fig. 39. Averaged vane torque vs. vane angle

5. Experimental validation of the model

The measurement of vane aerodynamic loading was performed using a high-pressure hot gas generator also called Gas Stand (see Fig. 40). This testing stand contains the hot gas generator, which generates a mixture of burned natural gas, and air at defined temperature and pressure. The pressure of the hot gas at the outlet of this device is controlled by the mass flow rate and the gas temperature. The whole testing stand provides a very precise measurement of flow thermodynamic properties. The main advantage of this device is that it excludes the influence of pressure pulsation, engine vibrations and engine control management. This enables testing under steady state conditions comparable to the CFD simulation.



Fig. 40. Gas Stand testing rig

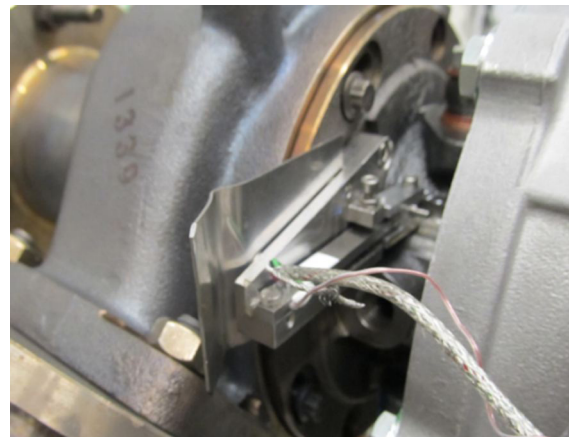


Fig. 41. Experimental device

6. Experimental device

A basic idea behind the aerodynamic loading measurement presented in this paper is a transfer of the aerodynamic torque acting on the vane to the bending moment of the load cell placed outside the turbine housing. A simple experimental device was developed for this purpose; its layout is presented in Fig. 42.

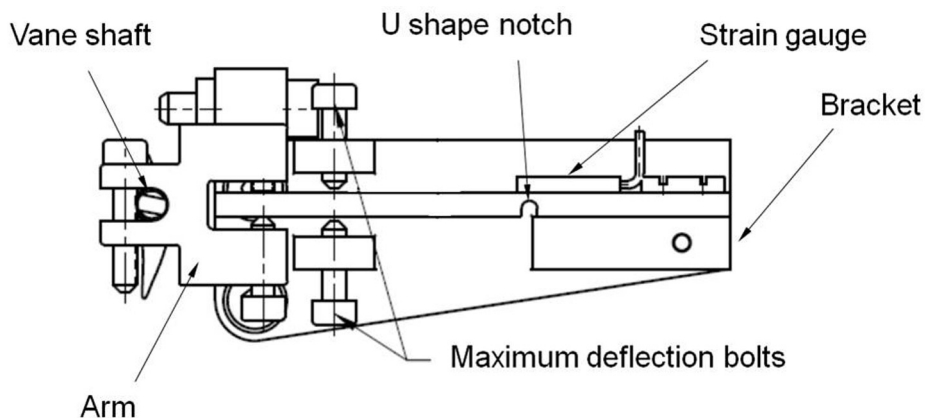


Fig. 42. Experimental device layout

The vane number nine was separated from the VNT assembly and its shaft was led out from the turbine housing. This is supported by two small ball bearings allowing the vane free rotation and minimizing the friction losses. The shaft is locked to a small arm using the screw lock

joint. This arm transfers the rotation movement of the vane to the bending moment of the load cell. This consists of the beam equipped with the strain gauge. A U-shape notch was used to multiply the loading and to increase sensitivity of the measurement. Deformation of the strain gauge is directly proportional to the acting aerodynamic torque. The load cell was attached to the supporting solid bracket and the whole device was mounted to the central housing (see Fig. 41). Calibration of the load cell was done using precise weights. The whole device was controlled and monitored using a LAB VIEW code. Three different vane positions were selected to cover the whole angular range of the vane. A simple protractor device was used to ensure the same angular position of the measured vane with the rest of them. This consists of precisely machined grooves for the vane shaft and the position holes for each of the selected vane angular positions. The protractor kept the vane in desired position before the measurement and then was removed to allow a transfer of the aerodynamic torque to the load cell. The strain gauge sensitivity range converted to the vane torque is from 0 to 100 Nmm, with the resolution of ± 0.5 Nmm. A compensated temperature range of the strain gauge is from 15 to 72 °C; thus the active cooling system was installed. This system consists of the pressed air nozzle and the small heat shield from the turbine side. Temperature of the load cell was monitored by the thermocouple during the whole measurement.

7. Measurement

The mass flow rate for each of the vane positions was calibrated to achieve the same turbine inlet pressure as that during the full load engine curve. Two decreased mass flow rates (-10% and -20%) are also investigated to extend the testing into the partial loading area. Measurements were repeated five times to ensure repeatability of results. The boundary conditions for the nine testing points are summarized in Table 2.

Table 2. Gas Stand boundary conditions

Configuration	Vane angle [deg]	Turbine inlet pressure [Pa]	Turbine inlet temperature [°C]	Turbine stage mass flow rate [$\text{kg} \cdot \text{s}^{-1}$]	Turbine outlet pressure [Pa]	Turbine wheel ω [$\text{rev} \cdot \text{min}^{-1}$]
Min open 1	84.66	259 000	490	0.046 45	98 300	38 900
Min open 2	84.66	286 000	500	0.050 19	98 240	41 760
Min open 3	84.66	331 000	491	0.058 62	98 240	47 120
Mid open 1	61.62	188 000	404	0.170 16	98 000	81 550
Mid open 2	61.62	205 000	401	0.189 01	98 150	88 800
Mid open 3	61.62	217 000	403	0.201 09	98 060	93 070
Max open 1	40.78	154 000	401	0.210 65	97 700	75 700
Max open 2	40.78	168 000	403	0.238 12	97 550	83 140
Max open 3	40.78	186 000	405	0.268 97	97 350	90 770

The main restriction of the measurement device is the maximum temperature which could be handled by the bearing system. This is made from stainless steel and the recommended maximum operating temperature is up to 150 °C. This results in restriction of the turbine inlet temperature to the 500 °C. There were no problems with bearing system observed during the test; however after cooling down, the sticking problem of the whole system appeared. This was probably caused by thermal degradation of the bearing material. Replacement of the bearing system after each cool down was necessary to avoid this effect. The solution in future work would be to use ceramic ball bearings which could stand much higher temperatures.

8. Evaluation of results

The results of the vane aerodynamic torque measurement for the vane number nine are summarized in Fig. 43. The maximum of the vane torque is in min open position; this is caused by a significantly higher pressure ratio as for the max open position (see Table 2). The vane number nine is strongly influenced by the spacer pin, which is visible from the torque reversal effect at mid open position. This is perfectly aligned with simulation results above (see Fig. 22).

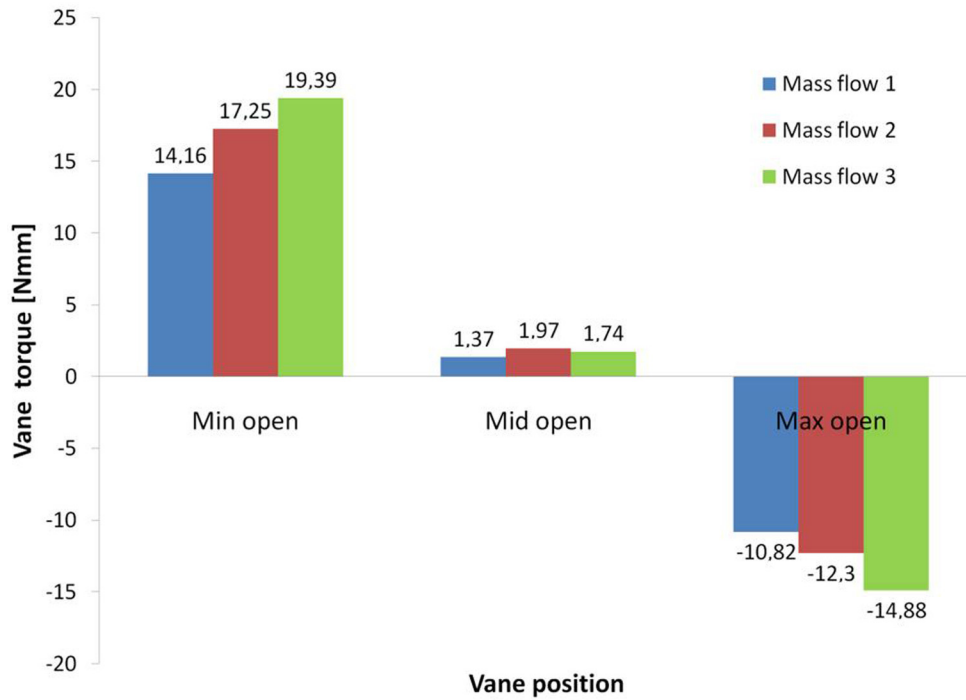


Fig. 43. Vane aero torque experimental results

All nine measured points were recalculated using pressure boundary conditions specified in Table 2. The comparison of the simulated and the measured aerodynamic torque values for the vane number nine is presented in Figs. 44–46. The second compared variable is the calculated turbine stage mass flow rate; this is presented in Fig. 47.

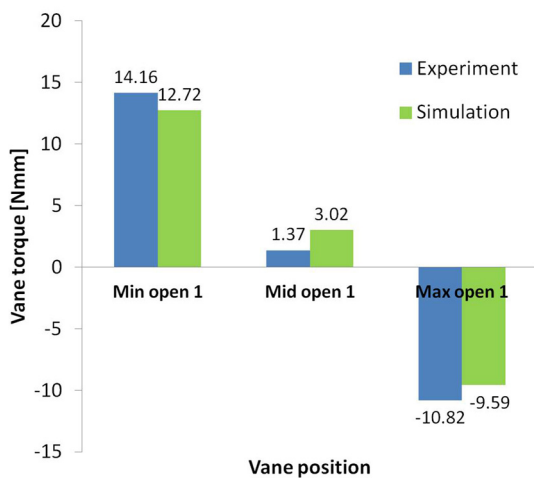


Fig. 44. Vane aero torque comparison (mass flow 1)

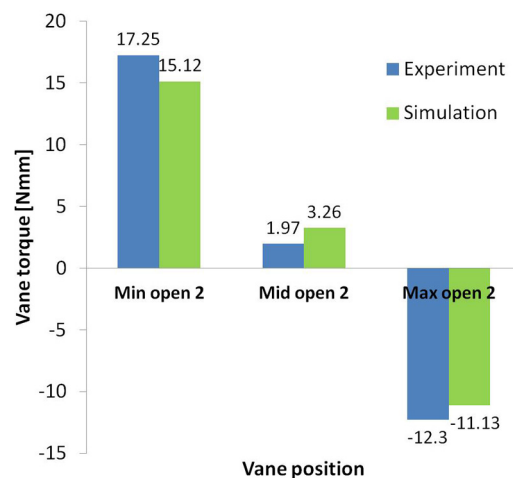


Fig. 45. Vane aero torque comparison (mass flow 2)

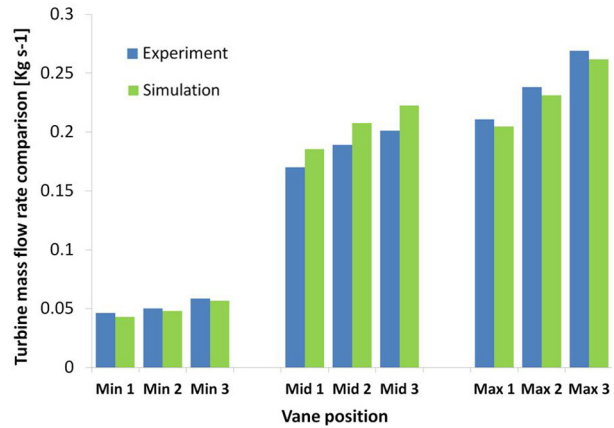
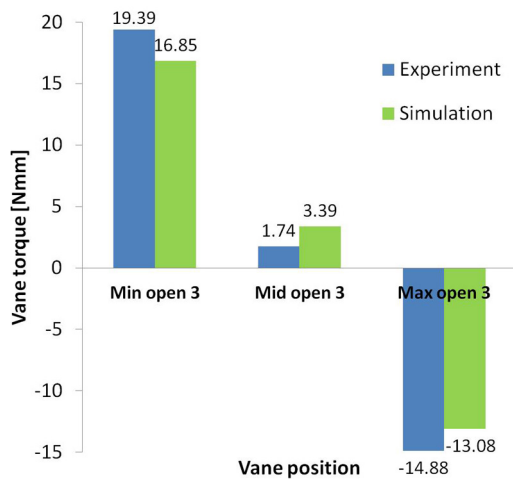


Fig. 46. Vane aero torque comparison (mass flow 3) Fig. 47. Turbine stage mass flow rate comparison

9. Conclusions

The calculation of vane aerodynamic loading offers a very good correlation with measured values. Trends are the same for all vane positions and mass flow rates. Differences at mid and max open positions are less than 1.7 Nmm. However, a min open position indicated a higher relative difference, up to 15 %. The explanation for this effect could be the difference between the relative vane to vane position of the measured vane and the rest of vanes. The measured vane is separated from the mechanism and set up during cold conditions without loading. However, after the test starts up, the whole mechanism tends to sit on the guiding elements and to consume internal plays. It means that the final relative vane to vane position could be slightly different, which influences the value of resulting vane torque.

The comparison of turbine mass flow rate presented in Fig. 47 also shows a good correlation with measured values with difference less than 10 %. These encouraging results show a high potential of CFD methods for further development and optimization of VNT mechanism.

Acknowledgements

This work was supported by Kinematics Science department of the Honeywell, Inc.

Reference

- [1] Baines, N. C., Lavy, M., Flows in vaned and vaneless stators of radial inflow turbocharger turbines, Institute of Mechanical Engineers Turbochargers and Turbocharging Conference, Paper No. C405/005, 1990, pp. 7–12.
- [2] Cetkovský, M., Turbocharger regulating VNT mechanism load simulation, Master thesis, Faculty of Mechanical Engineering, University of Technology in Brno, Brno, 2009.
- [3] Drdla, A., CFD simulation of turbocharger regulating mechanism, Master thesis, Faculty of Mechanical Engineering, University of Technology in Brno, Brno, 2010.
- [4] Menter, F. R., Two-equation eddy-viscosity turbulence models for engineering applications, *AIAA Journal* 32 (8) (1994) 1 598–1 605.
- [5] Simpson, A. T., Spence, S. W., Watterson, J. K. A., Comparison of the flow structures and losses within vaned and vaneless stators for radial turbines, *Journal of Turbomachinery* 131 (3) (2009), doi:10.1115/1.2988493.
- [6] Watson, N., Janota, M. S., Turbocharging the internal combustion engine, New York, Wiley, 1982.